ELSEVIER

Chemical Physics 261 (2000) 439–448

Chemical Physics

www.elsevier.nl/locate/chemphys

Graphite intercalation by nitric acid: conduction ESR and theoretical studies

A.M. Ziatdinov *, P.G. Skrylnik

Institute of Chemistry, Far Eastern Branch of the Russian Academy of Sciences, 159, Prospect 100-letiya, 690022 Vladivostok, Russian Federation

Received 21 February 2000; in final form 21 June 2000

Abstract

Results of an in situ conduction ESR (CESR) study of HNO_3 molecules intercalation into narrow highly oriented pyrolytic graphite (HOPG) slab are presented. The changes in the graphite CESR signal line shape, intensity and line width and the stepwise changes both of intensity and line width of CESR signal from intercalated sample have been clearly detected during this reaction. Under the assumption that the graphite CESR signal evolution is caused by the advance of a boundary separating the intercalated and non-intercalated HOPG, the average probability value of spin reorientation during the collision of current carriers with this interface and the constant of two-dimensional diffusion of nitric acid molecules into HOPG were extracted from experimental data. Using the dependence of chemical potential on exposure time of graphite in HNO_3 atmosphere offered by the authors for the experimental conditions, the stepwise evolution of CESR signal intensity from intercalated HOPG was calculated theoretically.

Keywords: Graphite; Intercalation; Conduction ESR; HNO_3

1. Introduction

In spite of numerous publications devoted to studies of various aspects of graphite intercalation compounds (GICs) structure and properties [1–3], hitherto many aspects of mechanism of "guest" molecules intercalation into graphite have not received sufficient attention. Conduction ESR (CESR) technique is one of the most powerful methods for studying the graphite intercalation process, because shapes and intensities of the CESR signal both from non-intercalated and intercalated regions of graphite plate vary strongly during the intercalation. However, because of the difficulty of similar experiments only a few CESR studies of graphite intercalation process have been undertaken [4–9]. But even in these cases, as a consequence of skin effect the interpretation of the changes in the graphite CESR signal during the intercalation process comes across greater difficulties. This paper is devoted to the results of an in situ CESR study of HNO_3 molecules intercalation into narrow highly oriented pyrolytic graphite (HOPG) slab (with basal plane width being comparable with the skin depth δ_c governed by the graphite c-axis conductivity σ_c). The results of theoretical analysis of the origin of (1) the stepwise

* Corresponding author. Tel.: +7-4232-311-655; fax: +7-4232-311-889.

E-mail address: chemi@online.ru (A.M. Ziatdinov).

0301-0104/00/$ - see front matter
PII: S0301-0104(00)00190-7

evolution of the CESR signal intensity from intercalated part of HOPG slab and (2) the increase of graphite CESR signal line width during the intercalation process, are also presented.

2. Experimental

CESR measurements were carried out at room temperature using an X-band E-line spectrometer. The constant magnetic field ($\mathbf{H}_0$) modulation frequency and amplitude were 2.5 kHz and 0.1 mT, respectively. The experiments were carried out on HOPG plates with height $(h) \times$ width $(l) \times$ thickness $(d) = 0.4 \times 0.04 \times 0.02$ cm^3, where $h \times l$ are the dimensions of basal plane. The HOPG samples were held in a quartz tube connected via a valve to the reservoir with intercalate (liquid HNO_3 with density $\rho \cong 1.565$ g/cm^3). Nitric acid vapors penetrated into the knee of reactor with the graphite sample through the hole with the size $\approx 8 \times 10^{-3}$ cm^2 in the fluoroplastic diaphragm. Prior to the experiment, the system was evacuated to eliminate air and water. During the measurements, $\mathbf{H}_0$ was applied along the graphite c-axis. The basal $l \times h$ and lateral $d \times h$ sides were parallel to the magnetic component ($\mathbf{H}_{rf}$) of the microwave field (Fig. 1). Note, that in the rectangular resonator the structure of electromagnetic field of TE_{102} mode has such a form that, at a conventional setting of the resonator, $\mathbf{H}_0$ is parallel to the electrical component ($\mathbf{E}_{rf}$) of microwave field (Fig. 1).

According to data of the four-probe method, at 300 K, the σ_c conductivity of HOPG plate used is equal to $(7.7 \pm 0.8)\ \Omega^{-1}\,\mathrm{cm}^{-1}$. In the X-band experiment, the value $\delta_c \sim l/2$ corresponds to this conductivity, i.e., the whole volume of the HOPG plate investigated was available for the CESR studies.

3. Results

The CESR spectrum of HOPG plate consists of single asymmetric line determined by Dyson mechanism [10]. The spectrum is axial with respect to the c-axis and is characterized by $g_{\|} = 2.0474 \pm 0.0002$ and $g_{\perp} = 2.0029 \pm 0.0002$. The line asymmetry parameter, A/B, being determined as the maximum/minimum peak height ratio, both measured with respect to the base-line of the first derivative of CESR absorption line, is 'normal' in the sense that the maximum peak occurs at the lower magnetic fields and it is equal to ≈ 1.8. In HOPG samples with $l \gg \delta_c$, the value of A/B is equal to $\cong 4$, i.e., it is essentially 'metallic'. Small value of A/B for the HOPG plate in our experiment is caused by the fact that CESR lineshape tends to Lorentzian with $A/B = 1$ at $l \to 0$.

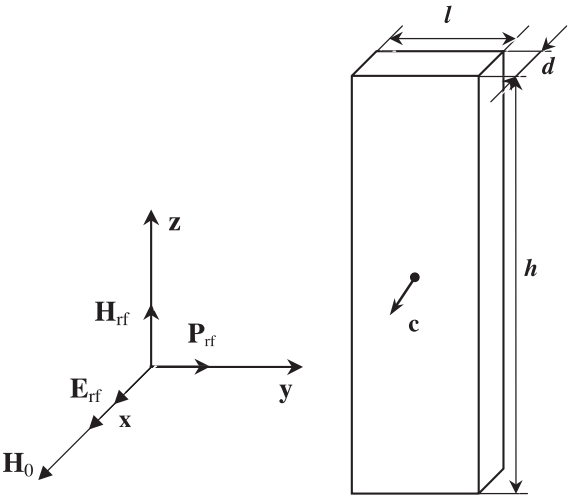

Fig. 1. The orientation of the HOPG plate with respect to the external magnetic field $\mathbf{H}_0$ and the cavity axis. $\mathbf{H}_{rf}$, $\mathbf{E}_{rf}$ and $\mathbf{P}_{rf}$ are the magnetic and electric components of the radio-frequency field, and the Poynting vector in an unloaded rectangular cavity.

Several minutes after the injection of HNO_3 gas into the part of reactor with the HOPG plate, the CESR signal of graphite begins to transform and decrease in intensity until it fully disappears (Fig. 2a). Simultaneously, a new signal with $g^*_{\|} = 2.0019 \pm 0.0002$, and $g^*_{\perp} = 2.0030 \pm 0.0002$ appears in the spectrum (Fig. 2b), where g^*_i $(i = \|, \perp)$ is determined by the H_0 value at the point of intersection of the first derivative of CESR absorption line and the base line.

The line width (the intensity), ΔH $(I = (A + B)\Delta H^2)$, of the graphite CESR signal increases (decreases) vs. exposure time, τ, monotonously (Fig. 2a). The A/B ratio of signal increases

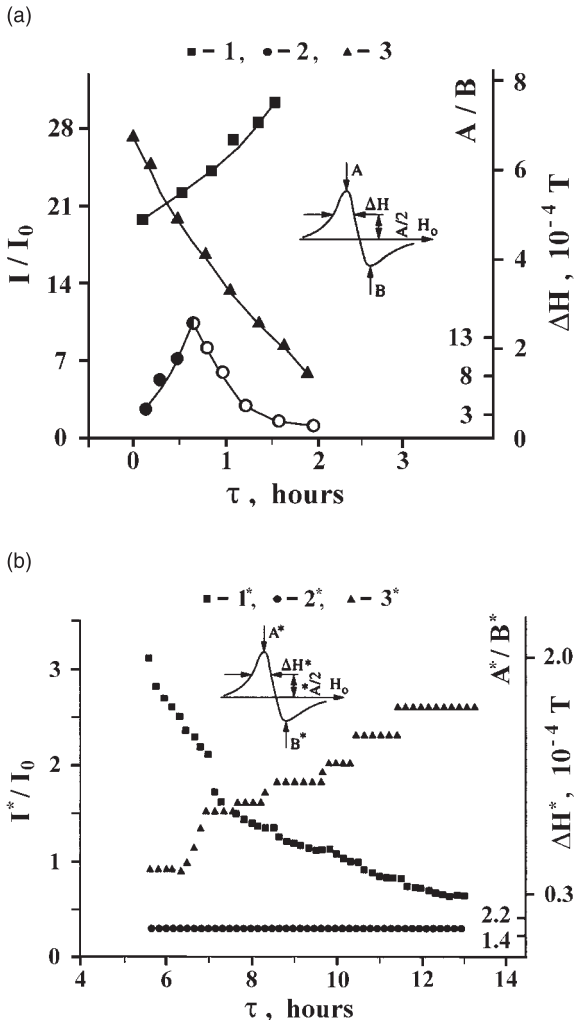

Fig. 2. CESR line shape parameters for (a) non-intercalated and (b) intercalated parts of the narrow ($l \sim 2\delta_c$) HOPG plate vs. exposure time, τ, in HNO_3 atmosphere. 1(1*), 2(2*) and 3(3*) correspond to ΔH (ΔH^*), A/B (A^*/B^*) and I/I_0 (I^*/I_0), respectively ($I[I^*] = (A+B)\Delta H^2[(A^*+B^*)\Delta H^{*2}]$; I_0 is the intensity of the Mn^{2+} ESR signal of the standard sample ($ZnS:Mn^{2+}$); the X-band; $T = 300$ K). In (a) the shaded and open dots are referred to the normal and 'reversed' line shape, respectively; half-shaded dot corresponds to the line shape with symmetric phase with respect to the A peak.

initially, but it is still 'normal' reaching a maximum value of $A/B \approx 13$. Later, upon further exposure in the intercalate atmosphere, the A/B ratio becomes 'reversed' (maximum peak, A, occurs at higher magnetic fields than the peak B), and its magnitude decreases down to ≈ 2; the A/B maximum corresponds to the moment when the phase reversal takes place (Fig. 2a). The g_i ($i = \|, \perp$) values of graphite CESR signal do not change up to its disappearance.

At the beginning of the reaction, a large scattering of the intensity, $I^* = (A^* + B^*)\Delta H^{*2}$, and the line width, ΔH^*, values of CESR signal with g_i^* has been observed. As τ increases, this scattering decreases and both the $I^*(\tau)$ and $\Delta H^*(\tau)$ dependences take a well-marked stepwise form (Fig. 2b). The asymmetry ratio, A^*/B^*, and g_i^* values of signal remain constant up to the end of reaction.

4. Discussion

With the configuration of our ESR experiment (Fig. 1), the microwave field penetrates into the HOPG plate mainly through its lateral sides, which are parallel to both the c-axis and $\mathbf{H}_{rf}$ [11], i.e. through the lateral sides $h \times d$. Therefore, the evolution of graphite CESR signal of the sample investigated (Fig. 2a) is mainly due to variations of the composition and properties of the HOPG plate at the surface areas from these sides. The dependence of the shape and intensity of graphite CESR signal on exposure time of a sample in HNO_3 vapors is qualitatively identical to that of the ESR signal line shape and intensity of the localized spins in a metallic substrate on the thickness of a spray-coated film of another metal [12]. In our case, the spins in consideration are certainly mobile, but for $l/\delta_c < 2$ the CESR line shape does not depend on spin mobility [13,14], i.e., in the framework of the Dyson theory [10] in HOPG plate investigated the spin carriers may be considered as localized. Therefore, the variations of the shape and intensity of the graphite CESR signal may be considered as caused by the formation of a macroscopic 'intercalation' layer on the HOPG substrate, and by the advance of the boundary which separates the intercalated and still not intercalated parts of sample. The invariability of g_i and g_i^* ($i^* = \|, \perp$) values up to the disappearance of graphite CESR signal and the end of reaction, respectively, indicates that the boundary may be considered as non-conductive. This may be

determined by significant distortion of a carbon net near the intercalation front and/or by the presence of high phase-boundary electrostatic potential.

In the experiment under consideration, the whole volume of sample investigated is available for CESR studies. Therefore, the time of the graphite CESR signal disappearance corresponds approximately to the moment of contact of the counter (antiparallel) intercalation fronts. Let us assume, that the intercalation is determined by a two-dimensional diffusion-controlled process, i.e., the thickness of the intercalated layer, d^*, depends on the exposure time as $(d^*)^2 = 2D_{\text{int}}\tau$, where D_{int} is intercalate two-dimensional diffusion constant. In such a case, having substituted the value of time interval from the beginning of the graphite CESR signal transformation up to its disappearance, $\tau \cong 3$ h, and $d^* = l/2$ to this expression, it is easy to estimate the value $D_{\text{int}} \cong 1,8 \times 10^{-12}$ m^2 s^{-1}. It is worth to note that this value of D_{int} well correlates with that obtained by high-resolution neutron scattering by Simon et al. [15]: $D_{\text{int}} \cong 4 \times 10^{-12}$ m^2 s^{-1}.

A new and unexpected result of this experiment is the significant broadening of the graphite CESR signal from the beginning of the intercalation up to the contact of the counter intercalation fronts (Fig. 2a). We suppose that the reason for it is the collisions of current carriers with the non-conductive boundary between the intercalated and the non-intercalated parts of the HOPG plate. Indeed, when the intercalation front advances inside a plate the width of its non-intercalated part decreases and, therefore, the frequency of collisions of spin carriers with the aforementioned interfaces increases. Therefore, assuming the probability of spin reorientation during such collisions to be different from zero, the increase of the total rate of spin relaxation of current carriers (the CESR line width) with the time of intercalation can be observed. Note that in all previous ESR experiments on graphite intercalation [4–9] which were carried out on HOPG plates with $l \gg \delta_c$, no broadening of the graphite CESR signal was observed. This indirectly supports our interpretation of the graphite CESR signal broadening at the intercalation of the narrow ($l \sim 2\delta_c$) HOPG plate. (The widening of the CESR signal from the intercalated graphite at the lowering of temperature [16–18] and at the disordered–ordered (liquid–solid) transformation of the HNO_3 layer near 250 K [16–18] is of different nature and, therefore, is not discussed in this paper.)

Using the relation $(d^*)^2 = 2D_{\text{int}}\tau$, the experimental dependence $\Delta H(\tau)$ (Fig. 2a) can be easily transformed into the dependence $\Delta H(a)$, where $a = l - 2d^*$ is the thickness of the non-intercalated part of HOPG plate (Fig. 3). The latter dependence can be calculated theoretically as well, using the Dyson theory for the CESR in metals, including the effects of surface relaxation [10]. It is assumed in this theory that an electron colliding with the surface has a certain probability ε of spin reorientation, in addition to the steady probability $1/T_2$ (T_2 is the spin-relaxation time due to the

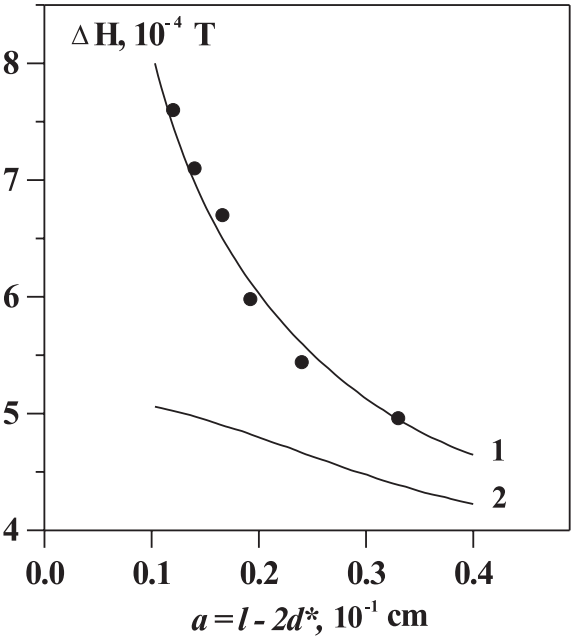

Fig. 3. Graphite CESR line width, ΔH, vs. thickness of the non-intercalated part of HOPG plate: $a = l - 2d^*$. The dots correspond to the experimental data. The lines 1 and 2 correspond to the theoretical graphite CESR linewidth calculated using the Dyson expression [10] with $G = 10$ and 0 cm^{-1}, respectively. The values of $R_a = 2.4$, $\delta_c = 2.6 \times 10^{-2}$ cm and $T_2 = 1.4 \times 10^{-8}$ s for HOPG plate intercalated, which are necessary for calculation of this theoretical dependences, were taken from Ref. [19].

collisions of current carriers with the imperfections in the sample volume) which exists for all electrons. In the general Dyson expressions for CESR line shape [10], the contribution of the surface spin relaxation effects to the CESR line shape is determined by the value of the term $Q = 1/2G\theta$, where $G = 3\varepsilon/4\Lambda$ (Λ is the mean free path of current carriers) and θ is the sample thickness. (The analysis of the mentioned Dyson expressions has shown that at given sample thickness the CESR line width increases with parameter G value. For $G \neq 0$, the value of CESR line width tends to the infinity at $\theta \to 0$.) Obviously, if ε is considered as an average value of probability of spin reorientation during collisions of graphite current carriers with the non-conductive phase boundary, then the mentioned expressions can be used for analysis of $\Delta H(a)$ dependence also. It is shown in Fig. 3, where the results of such analysis are presented, that the theoretical dependence of the graphite CESR line width with $G = 10$ cm^{-1} describes the experimental data well. (The HOPG values of $T_2 = 1.4 \times 10^{-8}$ s, T_{Da} (the spin diffusion time for diffusion along the graphite basal plane across the skin depth $\delta_c) = 8 \times 10^{-8}$ s and $\delta_c = 2.6 \times 10^{-2}$ cm, which are necessary for the calculation of this dependence, were taken from Ref. [19].) The resultant value of G and the typical HOPG values of $\Lambda = (0.4\text{–}1.6) \times 10^{-5}$ cm [20] correspond to $\varepsilon = (0.5\text{–}2.1) \times 10^{-4}$. It is worth noting that at present there are no data on interface spin relaxation in conductors in literature. There are only some published data on surface spin relaxation in simple metals. For comparison, the surface spin reorientation probabilities of conduction electrons in Cu and Li bulk samples are equal to $\sim 10^{-2}$ [21] and $\sim 5 \times 10^{-6}$ [22], respectively.

Experimental data (Fig. 2b) show that intercalation process is not a continuous one, i.e., it has clear stepwise shape: relatively short time intervals with sharp increase in I^* followed by the time intervals with I^* being near constant. This fact is in a good agreement with known literature data [1,23–29] reporting that in many cases the graphite intercalation proceeds through the formation of definite intercalation stages and that amount of intercalate inside the sample and, as a result, current carriers concentration, increases when the GIC stage index decreases. According to our X-ray diffraction data, the first (last) 'plateau' in experimental dependence $I^*(\tau)$ (Fig. 2b) corresponds to the seventh (second) intercalation stage. Therefore, the number of steps in the $I^*(\tau)$ dependence is equal to the number of possible intercalation stages and the step-wise increase in I^* may be attributed to the sequence of stage transitions from the stages with large integer indices to the stages with small ones. (The presence of two close steps instead of one, corresponding to the sixth stage (Fig. 2b), may be related with the change in the stacking of graphite layers situated between the nearest intercalate layers. First, such a stacking transformation was observed in the second stage alkali-metal-intercalated graphite by X-ray scattering measurements [30]. In $C_{5n}HNO_3$ the stacking transformations were not investigated, but the difference in a stacking sequence in samples with even and odd stage indices was experimentally proved [31–33]. The energy barrier associated with large-scale sliding of carbon layers at the stacking transformation, and corresponding changes in electronic structure decrease when the stage index number decreases. This reason may account for the absence of doubling the number of steps corresponding to the stages with index $n < 6$ in the experiment considered (Fig. 2b). In the following calculations we neglected the splitting of the 'plateau' in $I^*(\tau)$ dependence corresponding to the sixth stage). Under the above mentioned understanding of the reason for the stepwise dependence of $I^*(\tau)$, the time intervals with invariable value of I^* correspond to the periods, during which the insertion of intercalate from gas phase into the GIC plate is negligible. At this time, the concentration of current carriers in carbon layers does not change, but the reorganization of intercalate subsystem continues. In particular, this is confirmed by the CESR line-width decrease within the $I^*(\tau)$ 'plateau' (Fig. 2b). The reorganization of the intercalate subsystem during the considered time intervals may consist of splitting and merging of intercalate islands, at simultaneous increase of their mean size, and in agreement with other necessary conditions for the next stage transition.

The most commonly used model for theoretical investigations of staging phenomena in GICs is the

Safran model [34], which is, in principle, an Ising model with long-range antiferromagnetic interaction in external magnetic field. In this model interaction between intercalate molecules is supposed to be repulsive for molecules sitting in different graphite interlayer spaces, and attractive for the neighboring ones in the same graphite interlayer space. Following the Safran idea [34], Alstrom [35] has applied an one-dimensional Ising model with the corresponding model Hamiltonian:

$$H = -\mathrm{sign}(\rho_0)\mu\sum_i \sigma_i + \frac{1}{2}\sum_{i\neq j} V_{ij}\sigma_i\sigma_j \qquad (1)$$

to the investigation of stage phenomena in GICs. Interplanar repulsion of intercalate layers was introduced as $V_{ij} = 1/2V|i-j|^{-\alpha}$ (V is some constant depending on the total charge transfer between intercalant and graphite layer, α is an integer number related to the distribution of charge over the intervening graphite planes, i and j are layer indices). In Eq. (1), $\sigma_i = 1$ if an intercalate layer in the i'th graphite interlayer space exists and $\sigma_i = 0$ if not; ρ_0 is the intercalate layer charge density, that is $+1$ for donor intercalation and -1 for acceptor intercalation; μ is chemical potential with respect to pure graphite. Alstrom's [35] approach consisted in using the analytical solution of Bak and Bruinsma [36] for the problem of determining the set of σ_i with minimizing this Hamiltonian. The solution constitutes a "devil's staircase" $R(\mu)$, where the rational number R is the fraction of graphite interlayer spaces filled with intercalate, which means that $R = 1/n$ corresponds to the stage with index n. Every R value (and corresponding stage) exists inside some stability interval $\Delta\mu$ of the chemical potential. This solution was used by Alstrom [35] to describe the experiment performed by Falardeau [24] on the relative thickness increase of GIC plate in the z direction, $\Delta d/d_0$, during intercalation with AsF_5:

$$\frac{\Delta d}{d_0} = \left(\frac{c}{c_0} - 1\right) R = 1,42R,$$

where c and c_0 are the lattice parameters of the first stage AsF_5-GIC and graphite, respectively (Fig. 4). Comparison of theoretical results with experiment was carried out under the assumption that the dependence of the chemical potential on reaction time τ is similar to a relaxation equation:

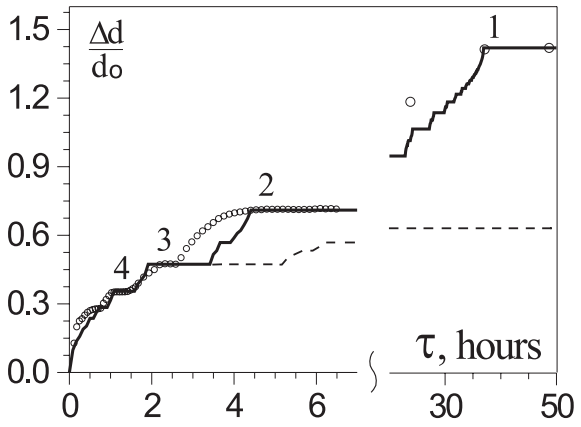

Fig. 4. c-Axis expansion ratio $\Delta d/d_0$ vs. reaction time τ for AsF_5-GIC (dots correspond to the experiment by Falardeau [24], dashed and solid lines correspond to Alstrom [35] and our theoretical calculations, respectively; stage indices are designated by the numbers).

$$\mu(\tau) = \mu_\infty(1 - \exp(-\tau/\tau^*)) \qquad (2)$$

with $\mu_\infty = -1.3$ eV, $\tau^* = 2.8$ h (Fig. 5). As Fig. 4 shows Alstrom's theoretical dependence $R(\tau)$ considerably differs from the experimental one: it never reaches stage 1 and 2 and the time interval

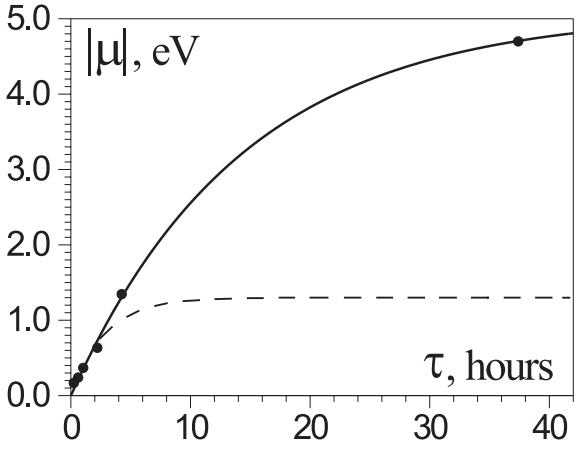

Fig. 5. Time dependence of the chemical potential μ (dots correspond to the experiment by Falardeau [24], dashed and solid lines correspond to Alstrom [35] and our theoretical calculations, respectively).

for stage 3 is very large [35]. It is worth noticing also that this method is based on the use of the theoretical dependence $R(\mu)$ for the *equilibrium* states (and stability intervals $\Delta\mu$ under equilibrium conditions) and subsequent transformation of $R(\mu)$ to $R(\tau)$ with some proposed dependence $\mu(\tau)$. From this it follows that application of the method of calculation is reasonable only for the cases with intercalation process being slow enough to be treated as a succession of equilibrium states. The advantage of the Alstrom's calculations [35] is the ability to qualitatively predict the stepwise dependence $R(\tau)$.

Another approach to the problem of intercalation process was proposed by Kirczenow [37]. This approach was based on computer simulation for intercalation kinetics and stage transitions with application of Monte-Carlo method using the Hamiltonian as follows:

$$H = \sum_i KN + \frac{1}{2}\sum_{i\neq j} Nu_{ij} + E_d, \tag{3}$$

where the summation is over the elementary islands of intercalate and N is the number of atoms (molecules) in the island. In Eq. (3), the first term is the Helmholtz free energy, second term is the interplanar repulsion energy of intercalate islands, third term is the dislocation energy corresponding to the edges of islands. The Kirczenow method [37] has the advantage that it allows to trace the intercalation process in microscopical scale (within the frameworks of some model) and to elucidate the qualitative features of this process. However, the disadvantage of the method comes from computational limitations which allow simulation for relatively small systems only, and necessity to solve a complex problem if chosen numerical method and Hamiltonian (and its parameters) correspond to the particular intercalation process under investigation.

In our paper for the theoretical interpretation of the observed experimental dependence $I^*(\tau)$ (Fig. 2b), analytical expressions for the stage fractions calculation by Kirczenow [38] (model of stage order and disorder as a result of the evolution of Daumas–Herold domains during intercalation process) have been utilized. In the frameworks of that model the calculation for the stage fractions f_i at given parameters (temperature, chemical potential, domain size etc.) may be fulfilled as follows [38]:

$$f_i = \exp(c_i) \quad \left(\sum_i \exp(c_i) = 1\right), \tag{4a}$$

$$c_i = N_0 \ln N_0 - N \ln N - (N_0 - N)\ln(N_0 - N) - \frac{\mathrm{i}\Psi}{kT} + \frac{1}{kT}\left(\mu N + \frac{\varepsilon z N^2}{2N_0} - \gamma N_0 - \frac{u_i N^2}{N_0}\right). \tag{4b}$$

Expression (4b) was found from the minimization of the free energy Ψ with respect to the distributions f_i and in-plane density x of intercalate within domain ($x = N/N_0$). In Eq. (4b), N_0 is the number of lattice-gas sites available to the intercalant in any graphite interlayer space within domain, N, the number of sites filled with intercalant, T, the temperature, k, the Boltzmann constant, μ, the chemical potential, ε, the nearest neighbor in-plane interaction energy between intercalants and, z, the in-plane coordination number, $u_i = v_0 i^{-\alpha}$, the repulsive interaction between intercalate layers across i carbon layers, γ, the energy per lattice-gas sites which is required to separate the host layers sufficiently to admit the intercalants. Having μ known and substituting other parameters to Eq. (4) we can obtain filling coefficient x and distribution f_i for the possible stages i. Then, resulting values let us estimate the total amount M of intercalant in GIC ($M_{\max}$ corresponds to the M value in pure first stage GIC):

$$M = M_{\max}\sum_i f_i\left(\frac{1}{i}\right)\frac{N}{N_0}. \tag{5}$$

In the experiment under consideration (the HOPG plate width $l \sim 2\delta_c$) CESR signal intensity I^* increases with the amount of intercalate molecules in the sample, i.e. $I^* \propto M$. The problem of choice for $\mu(\tau)$ dependence, which is necessary for the $I^*(\tau)$ calculation using Eq. (5), is a non-trivial one. In the present paper, following Alstrom [35], we have carried out the simulation of the intercalation process by introducing some dependence of

the chemical potential μ on time. It was supposed that during intercalation GIC system passes through a set of quasi-equilibrium states. Such assumption is supported by the following fact: in the considered experiment, intercalation process is slow enough and the lifetimes of definite stages greatly exceed the duration time of transitions between stages (Fig. 2b).

The reason for using in calculation of equilibrium states the analytical Eq. (4) by Kirczenow [38] instead of those by Alstrom [35] in the frameworks of "devil's staircase" model, is because Eq. (4) take into account the stage disorder phenomena. These phenomena are of importance in stage transitions [38], as confirmed by the numerical calculations of intercalation kinetics [37].

Basing on the foregoing qualitative consideration the following procedure has been used to obtain the dependence $\mu(\tau)$ corresponding to our experimental conditions. The threshold values of chemical potential μ_i, which correspond to the stage transitions from stages with indices $(i+1)$ to ones with indices i, were calculated with Eq. (4) theoretically. Corresponding threshold time values τ_i have been determined from experiment. The results of such calculations are presented in Fig. 6.

Before using in our analysis, the above procedure for determination of μ_i and τ_i was tested by applying to the aforementioned Alstrom treatment [35] of the Falardeau experiment [24]. Our calculations show that for the mentioned experiment the $\mu_i(\tau_i)$ dependence may be successfully fitted by the relaxation-like Eq. (2) (Fig. 5) but with different values of μ_∞ and τ^* (other parameters used were the same as in Ref. [35]). The subsequent calculation of $\Delta d/d_0(\tau)$ dependence for the Falardeau experiment [24] with new values of $\mu_\infty = -5.08$ eV and $\tau^* = 14.2$ h demonstrates more satisfactory agreement with the experimental dependence than those by Alstrom [35] (Fig. 4).

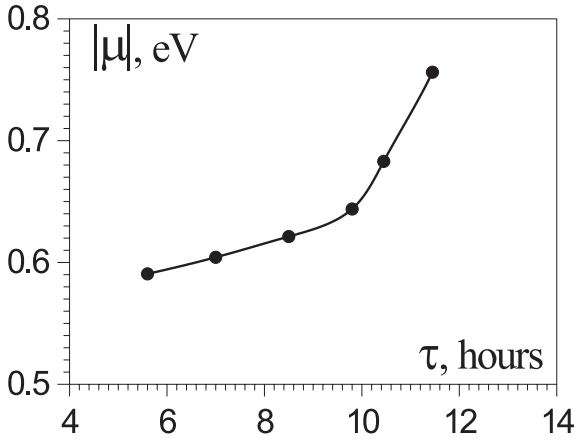

Fig. 6. Chemical potential of the narrow ($l \sim 2\delta_c$) HOPG plate, μ, vs. exposure time, τ, in HNO_3 atmosphere. Dots correspond to the threshold values μ_i and τ_i; solid line corresponds to the theoretical curve (Eq. (6)).

It is seen in Fig. 6 that for our experiment the dependence $\mu_i(\tau_i)$ qualitatively differs from adopted by Alstrom [35] Eq. (2). Probably, the reason for such deviation is the fact that aforementioned simple relaxation-like function is a good approximation for large exposure time only (see below). Therefore, we have used more general expression for $\mu(\tau)$ dependence:

$$\mu(\tau) = p'(\tau)\mu'(\tau) + p''(\tau)\mu''(\tau) \tag{6a}$$

$$\text{with} \quad \mu'(\tau) = a\tau^{\beta}, \tag{6b}$$

$$\mu''(\tau) = \mu_\infty(1 - \exp(-\tau/\tau^*)), \tag{6c}$$

where a and β are some real numbers, $p'(\tau)$ and $p''(\tau)$ are the weight functions, meeting the condition: $p'(\tau) + p''(\tau) \equiv 1$.

In Eq. (6a), the first term is dominant during the initial stages of intercalation, which are characterized by necessity of considerable pristine graphite deformation. The second term becomes dominant for the stages with low indices at the large time values. The formation of these stages requires large intercalate amount and, therefore, time. For these reasons functions $p'(\tau)$ and $p''(\tau)$ have been chosen as follows:

$$p'(\tau) = \exp(-\tau/\tau_0),$$

$$p''(\tau) = 1 - \exp(-\tau/\tau_0),$$

where τ_0 is the characteristic time, at which transition from one regime to another takes place. In our case (Fig. 2b), τ_0 is about 10 h. The calculation results for $I^*(\tau)$ in the frameworks of the above-stated model (with the set of parameters [38]:

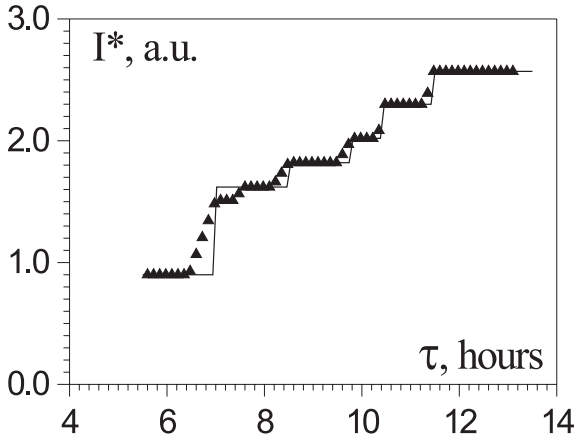

Fig. 7. The experimental (▲) and the calculated (—) integral intensity, I^*, of the CESR signal from intercalated HOPG plate vs. exposure time, τ, in HNO_3 atmosphere.

$N_0 = 300$, $z\varepsilon = 1$ eV, $\gamma = 1$ eV, $v_0 = 0.3$ eV, $\alpha = 1$) are shown in Fig. 7 and demonstrate a good agreement with experiment.

5. Conclusion

Graphite intercalation by HNO_3 molecules and stage transformations have been studied by CESR technique in narrow HOPG plate with width being comparable with the graphite skin depth governed by c-axis conductivity. As a result, the significant broadening of the graphite CESR signal during transport of the intercalate through the initial graphite sample and the stepwise changes in the intensity of the intercalated graphite CESR signal on exposure time in HNO_3 atmosphere have been clearly detected. Theoretical consideration for the time evolution of CESR parameters of signals both from non-intercalated and intercalated regions of sample has been carried out. A new form for the dependence of chemical potential vs. exposure time has been introduced with arguments presented, resulting in successful description of experimental dependence of CESR signal intensity from intercalated graphite. The broadening of graphite CESR signal during the advance of the intercalation front into the initial graphite sample has been explained by non-zero probability of spin reorientation during collisions of current carriers with the interface between the intercalated and the non-intercalated parts of the plate. Similar experimental and theoretical investigations of graphite intercalation by other intercalants are in progress.

Acknowledgements

The authors are grateful to N.M. Mishchenko, V.V. Sereda for their help in experiments and to L.B. Nepomnyashchii (Scientific Research Centre for Graphite, Moscow) for providing us with the HOPG. This work was supported by the Russian Foundation for Basic Research (Grant No. 00-03-32610).

References

[1] M.S. Dresselhaus, G. Dresselhaus, Adv. Phys. 30 (1981) 139.
[2] S.A. Solin, H. Zabel, Adv. Phys. 37 (1988) 87.
[3] P. Lagrange, A. Herold, C. Herold, Mol. Cryst. Liq. Cryst. 310 (1998) 33.
[4] R. Davidov, O. Milo, I. Palchan, H. Selig, Synth. Met. 8 (1983) 83.
[5] I. Palchan, D. Davidov, V. Zevin, G. Polatsek, H. Selig, Phys. Rev. B. 32 (1985) 5554.
[6] I. Palchan, F. Mustachi, D. Davidov, H. Selig, Synth. Met. 10 (1984/85) 101.
[7] M. Nakajima, K. Kawamura, T. Tsuzuku, J. Phys. Soc. Jpn 57 (1988) 1572.
[8] A.M. Ziatdinov, A.K. Tsvetnikov, N.M. Mishchenko, V.V. Sereda, Mat. Sci. Forum 91/93 (1992) 583.
[9] A.M. Ziatdinov, N.M. Mishchenko, J. Phys. Chem. Solids 58 (1997) 1167.
[10] F.J. Dyson, Phys. Rev. 98 (1955) 349.
[11] A.M. Ziatdinov, N.M. Mishchenko, Phys. Solid State Russia 36 (1994) 1289.
[12] V. Zevin, J.T. Suss, Phys. Rev. B. 34 (1986) 7260.
[13] H. Kodera, J. Phys. Soc. Jpn 28 (1970) 89.
[14] M. Saint-Jean, E. McRae, Phys. Rev. B. 43 (1991) 3969.
[15] C. Simon, I. Rosenman, F. Batallan, J. Rogerie, J.F. Legrand, A. Magerl, C. Lartique, H. Fuzellier, Phys. Rev. B. 41 (1990) 2390.
[16] S.K. Khanna, E.R. Falardeau, A.J. Heeger, J.E. Fischer, Solid State Comm. 25 (1978) 1059.
[17] P. Lauginie, H. Estrade, J. Conard, D. Guerard, P. Lagrange, M. El Makrini, Physica 99B (1980) 514.
[18] A.M. Ziatdinov, N.M. Mishchenko, Solid State Comm. 97 (1996) 1085.
[19] A.M. Ziatdinov, V.V. Kainara, A.N. Krivoshei, Mol. Cryst. Liq. Cryst. 340 (2000) 307.

[20] I.L. Spain, in: P.L. Walker, Jr., P.A. Throweer (Eds.), Chemistry and Physics of Carbon, Marcel Dekker, New York, 1973, vol. 8, p. 119.
[21] M.B. Walker, Phys. Rev. B. 3 (1971) 30.
[22] V.A. Zhikarev, A.P. Kessel, E.G. Harahashyan, F.G. Cherkasov, K.K. Shvarz, JETP USSR 64 (1973) 1356.
[23] D.E. Nixon, G.S. Parry, J. Phys. D. 1 (1968) 291.
[24] E.R. Falardeau, L.R. Hanlon, T.E. Thompson, Inorg. Chem. 17 (1978) 301.
[25] R. Nishitani, Y. Uno, H. Suematsu, Synth. Met. 7 (1983) 13.
[26] M.E. Misenheimer, H. Zabel, Phys. Rev. Lett. 54 (1985) 2521.
[27] R. Nishitani, Y. Nishina, S. Hashimoto, H. Iwasaki, Synth. Met. 12 (1985) 161.
[28] R. Nishitani, Y. Sasaki, Y. Nishina, J. Phys. Soc. Jpn 56 (1987) 1051.
[29] S.A. Safran, Solid St. Phys. 40 (1987) 183.
[30] M.J. Winokur, R. Clarke, Phys. Rev. Lett. 56 (1986) 2072.
[31] D.E. Nixon, G.S. Parry, A.R. Ubbelohde, Proc. Roy. Soc. London 291A (1966) 324.
[32] G.S. Parry, Mater. Sci. Engng. 31 (1977) 99.
[33] H. Shaked, H. Pinto, M. Melamud, Phys. Rev. B. 35 (1987) 838.
[34] S.A. Safran, Phys. Rev. Lett. 44 (1980) 937.
[35] P. Alstrom, Solid State Comm. 56 (1985) 1047.
[36] P. Bak, R. Bruinsma, Phys. Rev. Lett. 49 (1982) 249.
[37] G. Kirczenow, Phys. Rev. Lett. 55 (1985) 2810.
[38] G. Kirczenow, Phys. Rev. B. 31 (1985) 5376.